# EPR Spectroscopic and Theoretical Study of Chromium(I) Carbonyl Phosphine and Phosphonite Complexes

Derek A. Cummings, Jonathan McMaster, Anne L. Rieger, and Philip H. Rieger*

*Department of Chemistry, Brown University, Providence, Rhode Island 02912*

*Received March 24, 1997*[⊗]

Isotropic and frozen-solution EPR spectra are reported for several Cr(I) carbonyl complexes of the type *cis*-$[Cr(CO)_4L_2]^+$, *mer*- and *fac*-$[Cr(CO)_3L_3]^+$, and *trans*-$[Cr(CO)_2L_4]^+$, where L is a monodentate (or $L_2$ a bidentate) phosphine or phosphonite ligand. Extended Hückel molecular orbital theory calculations were performed for *cis*- and *trans*-$[Cr(CO)_4L_2]$, *mer*- and *fac*-$[Cr(CO)_3L_3]$, and *cis*- and *trans*-$[Cr(CO)_2L_4]$ (L = $PH_3$, $P(OH)_3$). The EPR results are discussed in light of the electronic structure predictions, which also provide some insights on the oxidation potentials and the isomerization reaction energetics of these complexes. Isotropic $^{31}P$ hyperfine couplings can be understood in terms of spin densities in the Cr 3d, P 3s, and P 3p orbitals.



## Introduction

Cr(0) and Cr(I) carbonyl phosphine, phosphite, and phosphonite complexes, $[Cr(CO)_{6-n}L_n]^{+/0}$, have been studied extensively,[1,2] with numerous reports of synthetic, electrochemical, and photochemical studies as well as IR, $^{31}P$ NMR, and EPR spectroscopic investigations.

Reported EPR spectra of $[Cr(CO)_6]^+$ [3,4] and *trans*-$[Cr(CO)_4(PPh_3)_2]^+$ [5] attracted our attention to the Cr(I) carbonyl phosphines. Ligand-field theory arguments[6] predict $^2T$ and $^2E$ ground states for these species; degenerate ground-state molecules are subject to dynamic Jahn−Teller distortions, so that EPR spectra should not be detectable much above liquid He temperature. Experimental results for the isoelectronic V(0) complexes are in complete accord with these predictions,[6,7] but the spectra assigned to $[Cr(CO)_6]^+$ and *trans*-$[Cr(CO)_4(PPh_3)_2]^+$ are almost certainly wrong, since spectra were recorded at or only a little below room temperature. Although several EPR studies have been reported for other Cr(I) carbonyl phosphines, they have been limited to isotropic, liquid-solution spectra and thus give little information about the detailed electronic structure of these complexes.

Extended Hückel molecular orbital (EHMO) theory calculations have been reported by Mingos[8] for several molybdenum analogs, and Bursten[9] has discussed ligand effects on the electrochemical oxidations and photoelectron spectra of octahedral complexes, but otherwise there has been no systematic attempt to correlate spectroscopic results with a theoretical understanding of electronic structure.

These species have been of interest in part because of the reactivity of the Cr(I) carbonyl phosphines, which are known to isomerize to the thermodynamically most stable isomer, disproportionate, or react with other ligands.[10,11] Much of the behavior of *cis*- and *trans*-$[Cr(CO)_4L_2]$,[12,13] *mer*- and *fac*-$[Cr(CO)_3L_3]$,[13,14] and *cis*- and *trans*-$[Cr(CO)_2L_4]$[15] can be understood in terms of the square schemes and electron-transfer cross reactions shown in Schemes 1−3, where in most cases $K_1 < 1$ and $K_2 >> 1$. Thus, oxidation of either a *mer*-$(CO)_3$ or *fac*-$(CO)_3$ complex gives *mer*$^+$ and oxidation of a *cis*-$(CO)_2$ or *trans*-$(CO)_2$ complex gives *trans*$^+$ as the final product. One of the goals of this work was to rationalize these results in terms of the electronic structure of the complexes.

We had hoped that the relatively sharp features of the frozen-solution EPR spectra of these complexes would permit accurate determination of the $\mathbf{A}^P$-matrices. With accurate measurements, we could estimate

[⊗] Abstract published in *Advance ACS Abstracts,* September 15, 1997.

(1) Kirtley, S. W. In *Comprehensive Organometallic Chemistry*; Wilkinson, G., Stone, F. G. A., Abel, E. W., Eds.; Pergamon: Oxford, U.K., 1982; Vol. 3.
(2) Bond, A. M.; Colton, R.; Cooper, J. B.; McGregor, K.; Walter, J. N.; Way, D. M. *Organometallics* **1995**, *14*, 49 and references therein.
(3) Pickett, C. J.; Pletcher, D. *J. Chem. Soc., Dalton Trans.* **1975**, 879.
(4) Bagchi, R. N.; Bond, A. M.; Colton, R.; Luscombe, D. L.; Moir, J. E. *J. Am. Chem. Soc.* **1986**, *108*, 3352.
(5) Bagchi, R. N.; Bond, A. M.; Brain, G.; Colton, R.; Henderson, T. L. E.; Kevekordes, J. E. *Organometallics* **1984**, *3*, 4.
(6) Rieger, P. H. *Coord. Chem. Rev.* **1994**, *135/136*, 203.
(7) (a) Pratt, D. W.; Myers, R. J. *J. Am. Chem. Soc.* **1967**, *89*, 6470. (b) Rubinson, K. A. *J. Am. Chem. Soc.* **1976**, *98*, 5188. (c) Boyer, M. P.; LePage, Y.; Morton, J. R.; Preston, K. F.; Vuolle, M. J. *Can. J. Spectrosc.* **1981**, *26*, 181. (d) Ammeter, J. H.; Zoller, L.; Bachmann, J.; Baltzer, P.; Gamp, E.; Bucher, R.; Deiss, E. *Helv. Chim. Acta* **1981**, *64*, 1063. (e) Bratt, S. W.; Kassyk, A.; Perutz, R. N.; Symons, M. C. R. *J. Am. Chem. Soc.* **1982**, *104*, 490. (f) McCall, J. M.; Morton, J. R.; Preston, K. F. *Organometallics* **1985**, *4*, 1272. (g) McCall, J. M.; Morton, J. R.; Preston, K. F. *J. Magn. Reson.* **1985**, *64*, 414.
(8) Mingos, D. M. P. *J. Organomet. Chem.* **1979**, *179*, C29.
(9) Bursten, B. E. *J. Am. Chem. Soc.* **1982**, *104*, 1299.
(10) Salt, J. E.; Wilkinson, G.; Motevalli, M.; Hursthouse, M. B. *J. Chem. Soc., Dalton Trans.* **1986**, 1141.
(11) Blagg, A.; Carr, S. W.; Cooper, G. R.; Dobson, I. D.; Gill, J. B.; Goodall, D. C.; Shaw, B. L.; Taylor, N.; Boddington, T. *J. Chem. Soc., Dalton Trans.* **1985**, 1213.
(12) Bond, A. M.; Colton, R.; Mann, T. F. *Organometallics* **1988**, *7*, 2224.
(13) Bond, A. M.; Colton, R.; Kevekordes, J. E. *Inorg. Chem.* **1986**, *25*, 749.
(14) (a) Bond, A. M.; Carr, S. W.; Colton, R. *Organometallics* **1984**, *3*, 541. (b) Bond, A. M.; Carr, S. W.; Colton, R. *Inorg. Chem.* **1984**, *34*, 2343. (c) Bond, A. M.; Colton, R.; McGregor, K. *Inorg. Chem.* **1986**, *25*, 2378. (d) Bagchi, R. N.; Bond, A. M.; Colton, R.; Creece, I.; McGregor, K.; Whyte, T. *Organometallics* **1991**, *10*, 2611. (e) Bond, A. M.; Colton, R.; Feldberg, S. W.; Mahon, P. J.; Whyte, T. *Organometallics* **1991**, *10*, 3320.
(15) (a) Bond, A. M.; Colton, R.; Jackowski, J. J. *Inorg. Chem.* **1975**, *14*, 2526. (b) Bond, A. M.; Grabaric, B. S.; Jackowski, J. J. *Inorg. Chem.* **1978**, *17*, 2153. (c) Bond, A. M.; Colton, R.; Cooper, J. B.; Traeger, J. C.; Walter, J. N.; Way, D. M. *Organometallics* **1994**, *13*, 3434.

S0276-7333(97)00252-5 CCC: $14.00 

**Scheme 1**

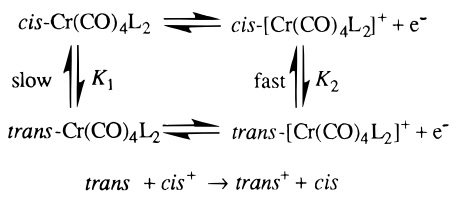


**Scheme 2**

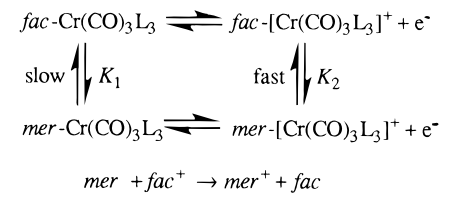


**Scheme 3**

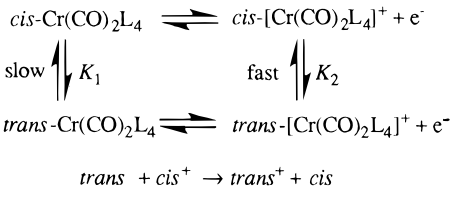


the phosphorus 3p contribution to the singly occupied molecular orbital (SOMO), thus obtaining a direct measure of $\pi$-back-bonding to phosphorus ligands. In this, we were disappointed; the accuracy of the results is not quite sufficient to permit such an analysis. The results do, however, provide some useful insights into the significance of isotropic $^{31}$P couplings.

In the following, we report isotropic and frozen-solution spectra of several Cr(I) carbonyl phosphine and phosphonite complexes and EHMO calculations on some model compounds. Electrochemical results and EPR parameters—**g**-matrices and isotropic $^{31}$P couplings—are discussed in light of the electronic structure predictions.

## Experimental Section

**Materials.** Chlorinated solvents were distilled from calcium hydride under nitrogen. Hydrocarbons were dried over sodium. Diethyl ether and tetrahydrofuran were distilled from sodium benzophenone ketyl under nitrogen. Methanol was distilled from $[Mg(OCH_3)_2]$ under nitrogen after predrying with molecular sieves. Triethylamine was distilled under nitrogen from 1-naphthyl isocyanate after predrying over sodium hydroxide. Other solvents were used as supplied.

$[Cr(CO)_6]$, $[(C_7H_8)Cr(CO)_3]$, $PPh_3$, $PMe_3$, $PPhMe_2$, $CH_3C(CH_2PPh_2)_3$ (triphos), $(Ph_2PCH_2)_2$ (dppe), $(Ph_2P)_2CH_2$ (dppm), and $PPh(OMe)_2$ were obtained from Aldrich or Strem. $[(MeO)_2PCH_2]_2$ (pompom) was prepared by the method of King and Rhee[16] from $Cl_2PCH_2CH_2PCl_2$ (Strem). It is absolutely essential to distill the reaction product and to rigorously exclude water and oxygen.

The Cr(0) complexes were prepared by literature methods or small variations thereof: $[Cr(CO)_4(PPh_3)_2]$ by the method of Chatt *et al.*,[17] *mer*-$[Cr(CO)_3\{PPh(OMe)_2\}_3]$, *fac*-$[Cr(CO)_3(PMe_3)_3]$, and *fac*-$[Cr(CO)_3(PPhMe_2)_3]$ by the method of Shaw,[18] *fac*-$[Cr(CO)_3\{CH_3C(CH_2PPh_2)_3\}]$ by the method of Ismail and Butler,[19] *mer*-$[Cr(CO)_3(\eta^2\text{-dppm})(\eta^1\text{-dppm})]$ by the method of Blagg *et al.*,[11] *cis*-$[Cr(CO)_2(dppe)_2]$ and $[Cr(CO)_4(dppe)]$ by the method of Zingales and Canziani,[20] and *cis*-$[Cr(CO)_2(pompom)_2]$ by the method of King and Rhee.[16] IR carbonyl bands were in agreement with literature values,[21] mass spectra gave the expected parent ion peaks, and electrochemical oxidation potentials matched those reported in the literature (see Table 2). In almost all cases, small amounts of paramagnetic impurities, usually the expected Cr(I) species, were detectable by EPR spectroscopy, even after repeated recrystallizations. All operations were performed under either argon using Schlenk techniques or a Vacuum Atmospheres drybox.

Solutions of the Cr(I) cations were prepared by chemical oxidation, using $[Cp_2Fe][BF_4]$ or $[4\text{-}O_2N\text{-}C_6H_4N_2][BF_4]$, of dilute (5−10 mM) solutions of the Cr(0) precursors or by *in situ* electrochemical oxidation at a Pt anode of Cr(0) solutions containing 0.1 M $[Bu_4N][ClO_4]$ or $[Bu_4N][PF_6]$. In either case the solvent was 1/1 $CH_2Cl_2$/1,2-$C_2H_4Cl_2$ or 2/1 THF/$CH_2Cl_2$.

**Instrumentation**. EPR spectra were obtained using a Bruker ER-220D X-band spectrometer equipped with a Bruker variable-temperature accessory, a Systron-Donner microwave frequency counter, and a Bruker gauss meter. Infrared spectra were recorded with a Mattson FT-IR spectrometer. Mass spectra were obtained with a Kratos MS80RFA spectrometer in positive-ion mode with fast atom bombardment using *m*-nitrobenzyl alcohol as a matrix. Cyclic voltammograms were obtained using EG&G Model 173/175/179 potentiostatic instrumentation. The working electrode was a 1 mm platinum or glassy-carbon disk, the counter electrode was a platinum wire, and the reference electrode was Ag/AgCl in contact with $CH_2Cl_2$/$[Bu_4N][ClO_4]$ saturated with LiCl. Ferrocene was used as an internal potential standard.

## Results

**EPR Spectra**. *trans*-$[Cr(CO)_2(dppe)_2]^+$, generated electrochemically, is long-lived at room temperature and gives well-resolved isotropic and frozen-solution spectra. The five-line isotropic spectrum shows $^{53}$Cr satellites, in agreement with that reported earlier.[15c] The frozen-solution spectrum, shown in Figure 1a, has resolved components for all three principal values of the **g**-matrix so that these parameters and the associated $^{31}$P couplings are measurable directly. Unfortunately, we were unable to resolve the expected $^{53}$Cr satellites in the frozen-solution spectra. *trans*-$[Cr(CO)_2(pompom)_2)]^+$, generated by $[Cp_2Fe]^+$ oxidation of the *cis* isomer, gives a very similar isotropic spectrum, but in the frozen-solution spectrum shown in Figure 1b, features corresponding to the middle **g**-component are unresolved. EPR parameters for these and other spectra are given in Table 1.

Isotropic and frozen-solution spectra of *mer*-$[Cr(CO)_3(PMe_3)_3]^+$, generated by electrochemical or $[O_2NC_6H_4N_2]^+$ oxidation of the neutral *fac* complex, are well-resolved, so that all parameters are easily measurable. Electrolysis of *fac*-$[Cr(CO)_3(PPhMe_2)_3]$ at 250 K gave the well-resolved isotropic spectrum of *mer*-$[Cr(CO)_3(PPhMe_2)_3]^+$ as a doublet of triplets, in agreement with the report by Bond *et al.*,[14b,22] although their EPR parameters are apparently erroneous. The frozen-solution spectrum closely resembles that of the $PMe_3$ analog but is less well-resolved. Rapid low-temperature $[Cp_2$-

(16) King, R. B.; Rhee, W. M. *Inorg. Chem.* **1978**, *17*, 2961.
(17) Chatt, J.; Leigh, G. J.; Thankarajan, N. *J. Organomet. Chem.* **1971**, *29*, 105.
(18) Jenkins, J. R.; Moss, J. R.; Shaw, B. L. *J. Chem. Soc. A* **1969**, 2796.
(19) Ismail, A. A.; Butler, I. A. *J. Organomet. Chem.* **1988**, *346*, 185.
(20) Zingales, F.; Canziani, F. *Gazz. Chim. Ital.* **1962**, *92*, 343.
(21) IR bands found for *mer*-$[Cr(CO)_3\{PPh(OMe)_2\}_3]$ were in agreement with those reported by Shaw and co-workers,[18] but not with those of Bond et al.[14b]
(22) Bagchi, R. N.; Bond, A. M.; Colton, R. *J. Electroanal. Chem. Interfacial Electrochem.* **1986**, *199*, 297.

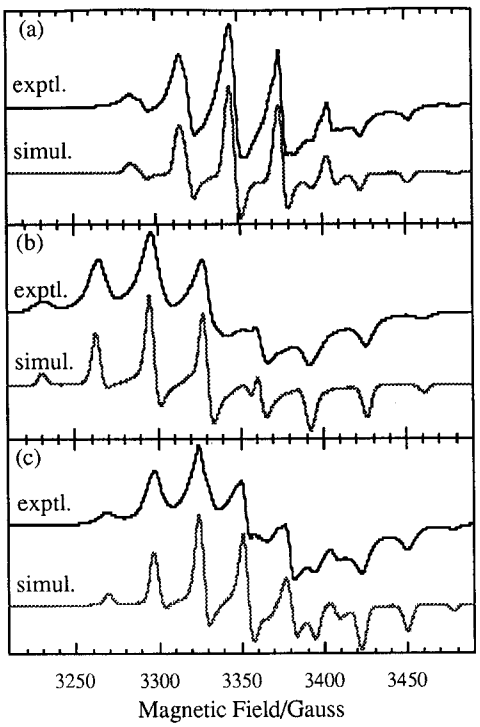


**Figure 1.** Experimental and computer-simulated X-band spectra of (a) *trans*-$[Cr(CO)_2(dppe)_2]^+$, (b) *trans*-$[Cr(CO)_2(pompom)_2]^+$, and (c) *trans*-$[Cr(CO)_2(dppm)_2]^+$. Experimental spectra were of $CH_2Cl_2/C_2H_4Cl_2$ solutions at 110 K; computer simulations used the parameters of Table 1 and Gaussian line shapes with $\sigma = 2.5$ G.

Fe]$^+$ oxidation of *fac*-$[Cr(CO)_3(PPhMe_2)_3]$, followed by immediate freezing of the solution, resulted in a different spectrum, which we assign to the *fac* cation; this spectrum rapidly converted to that of the *mer* cation on melting.[23]

Isotropic spectra of *mer*-$[Cr(CO)_3\{PPh(OMe)_2\}_3]^+$ and *mer*-$[Cr(CO)_3(\eta^2\text{-dppm})(\eta^1\text{-dppm})]^+$, generated by electrochemical oxidation, are approximate 1:3:3:1 quartets, as reported by Bond *et al.*[14b,d,22] The two central lines are somewhat broader than the outer lines, suggesting a poorly resolved doublet of triplets. Least-squares analyses[24] of these spectra gave reasonably good estimates of the two coupling constants. Frozen-solution spectra of these complexes were approximately axial, with coupling to three apparently equivalent $^{31}$P nuclei. When it stood at room temperature, the solution of *mer*-$[Cr(CO)_3(\eta^2\text{-dppm})(\eta^1\text{-dppm})]^+$ exhibited the five-line spectrum of *trans*-$[Cr(CO)_2(dppm)_2]^+$, as reported earlier.[11,25] The frozen-solution spectrum, shown in Figure 1c, is well-resolved so that all components of the **g**-matrix and the associated $^{31}$P couplings could be measured directly.

Attempts to generate *fac*-$[Cr(CO)_3\{CH_3C(CH_2PPh_2)_3\}]^+$ *in situ* by electrochemical oxidation failed. The cation was prepared by low-temperature oxidation with $[O_2NC_6H_4N_2][BF_4]$, followed by immediate freezing of the solution. The frozen-solution spectrum was axial, but the $g_\perp$ region was unresolved. The cation decayed rapidly at temperatures above 200 K, so that we were unable to obtain an isotropic spectrum.

$[Cr(CO)_4(dppe)]^+$, generated by electrochemical or $[O_2NC_6H_4N_2]^+$ oxidation, gives a nearly axial frozen-solution spectrum with the $g_\perp$ region poorly resolved. This cation is short-lived at room temperature, and we were unable to record an isotropic spectrum. The isotropic parameters computed from those in Table 1 are $\langle g\rangle = 2.05$ $\langle a^P\rangle = 23$ G, quite different from those reported for $[Cr(CO)_4(dppm)]^+$ by Bond, *et al.*,[26] $\langle g\rangle = 2.009$ and $\langle a^P\rangle = 6.9$ G). We have observed spectra with similar parameters, but always under circumstances where there was reason to suspect decomposition; the identity of the species responsible for these spectra remains unknown.

**Table 1. EPR Parameters[a]**

(a) Isotropic Parameters

| complex | $\langle g\rangle$ | $\langle A^P\rangle$[b] | $\langle A^{Cr}\rangle$ |
|---|---|---|---|
| *mer*-$[Cr(CO)_3\{PPh(OMe)_2\}_3]^+$ | 2.028 | 31.2 (1)<br>27.1 (2) | |
| *mer*-$[Cr(CO)_3(\eta^1\text{-dppm})(\eta^2\text{-dppm})]^+$ | 2.016 | 22.8 (1)<br>19.6 (2) | |
| *mer*-$[Cr(CO)_3(PMe_3)_3]^+$ | 2.024 | 28.0 (1)<br>21.5 (2) | 12.7 |
| *mer*-$[Cr(CO)_3(PPhMe_2)_3]^+$ | 2.022 | 27.0 (1)<br>19.7 (2) | |
| *trans*-$[Cr(CO)_2(dppm)_2]^+$ | 2.004 | 25.82 (4) | 14.2 |
| *trans*-$[Cr(CO)_2(dppe)_2]^+$ | 2.015 | 26.91 (4) | 14.6 |
| *trans*-$[Cr(CO)_2(pompom)_2]^+$ | 2.023 | 31.49 (4) | 12.8 |

(b) Anisotropic Parameters[c]

| complex | $g$ | $A^P$[b] | |
|---|---|---|---|
| $[Cr(CO)_4(dppe)]^+$ | 2.09 | 22 (2) | |
| | 2.08 | 22 | |
| | 1.988 | 22.8 | |
| *fac*-$[Cr(CO)_3(triphos)]^+$ | 2.080 | | |
| | 2.080 | | |
| | 1.994 | 21.3 (3) | |
| *fac*-$[Cr(CO)_3(PPhMe_2)_3]^+$ | 2.054[d] | 22[d] (3) | |
| | 2.054[d] | 22[d] | |
| | 1.988[d] | 26[d] | |
| *mer*-$[Cr(CO)_3(PPhMe_2)_3]^+$ | [2.042] | [31] (1) | [18] (2) |
| | 2.034 | 29 | 20 |
| | 1.989 | 21[e] | 21[e] |
| *mer*-$[Cr(CO)_3\{PPh(OMe)_2\}_3]^+$ | 2.048[e] | 29.5[d] (3) | |
| | 2.048[e] | 29.5[d] | |
| | 1.986[e] | 29.5[d] | |
| *mer*-$[Cr(CO)_3(\eta^1\text{-dppm})(\eta^2\text{-dppm})]^+$ | 2.034 | 24 (4) | |
| | 2.034 | 24 | |
| | 1.982 | 21.1 | |
| *mer*-$[Cr(CO)_3(PMe_3)_3]^+$ | [2.046] | [27.4] (1) | [20.4] (2) |
| | 2.034 | 29.7 | 21.9 |
| | 1.991 | 26.9 | 22.3 |
| *trans*-$[Cr(CO)_2(dppm)_2]^+$ | 2.031 | 26.4[e] (4) | |
| | 2.014 | 25.0 | |
| | 1.973 | 25.5 | |
| *trans*-$[Cr(CO)_2(dppe)_2]^+$ | 2.027 | 28.5[e] (4) | |
| | 2.025 | 26.8 | |
| | 1.980 | 26.5[d] | |
| *trans*-$[Cr(CO)_2(pompom)_2]^+$ | 2.049 | 31.1[d] (4) | |
| | [2.029] | [31.5] | |
| | 1.991 | 31.9[d] | |

[a] Hyperfine couplings in units of $10^{-4}$ cm$^{-1}$; uncertainties are $\pm 1$ in last digit unless otherwise noted. [b] Number in parentheses indicates number of $^{31}$P nuclei. [c] Values in brackets computed from measured components and the isotropic parameters. [d] Uncertainty $\pm 2$ in last decimal place. [e] Uncertainty $\pm 3$ in last decimal place.

(23) A similar attempt to obtain the spectrum of *cis*-$[Cr(CO)_2(dppe)_2]^+$ was not successful; only the *trans* isomer was obtained on low-temperature oxidation.

(24) Atkinson, F. L.; Blackwell, H. E.; Brown, N. C.; Connelly, N. G.; Crossley, J. G.; Orpen, A. G.; Rieger, A. L.; Rieger, P. H. *J. Chem. Soc., Dalton Trans.* **1996**, 3491.

(25) This and related rearrangement reactions are photochemical in nature and will be discussed in detail elsewhere.

(26) Bond, A. M.; Colton, R.; Kevekordes, J. E.; Panagiotidou, P. *Inorg. Chem.* **1987**, *26*, 1430−1435.

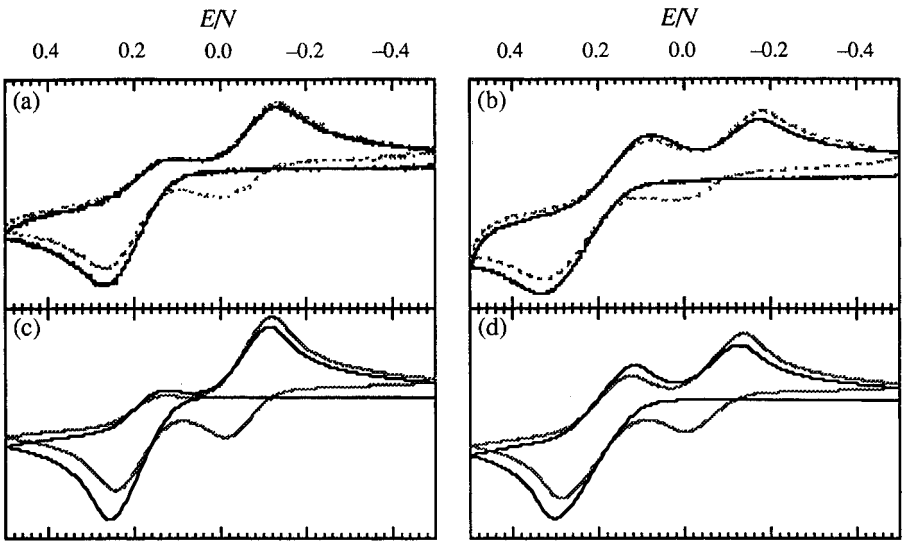


**Figure 2.** Cyclic voltammograms on glassy carbon of 1 mM *cis*-$[Cr(CO)_2(pompom)_2]$ in $CH_2Cl_2$ with 0.1 M $[Bu_4N][PF_6]$ at 20 °C (potentials vs Ag/AgCl). Experimental curves: (a) 0.5 V $s^{-1}$; (b) 2.0 V $s^{-1}$. Computer simulations with $k = 5.0$ $s^{-1}$: (c) 0.5 V $s^{-1}$; (d) 2.0 V $s^{-1}$.

**Table 2. Electrochemical Data for Cr Complexes in $CH_2Cl_2$**

| complex | $E_{1/2}$/V[a] | ref |
|---|---|---|
| *cis*-$[Cr(CO)_4(dppe)]$ (**1**) | 0.27 | 26 |
| *trans*-$[Cr(CO)_4(PPh_3)_2]$ (**2**) | 0.16 | this work |
| *fac*-$[Cr(CO)_3(triphos)]$ (**3**) | −0.09 | this work |
| *fac*-$[Cr(CO)_3(PPhMe_2)_3]$ (**4**) | −0.12 | this work |
| *mer*-$[Cr(CO)_3(PPhMe_2)_3]$ (**5**) | −0.49 | this work |
| *mer*-$[Cr(CO)_3[PPh(OMe)_2]_3]$ (**6**) | −0.20 | this work |
| *mer*-$[Cr(CO)_3(\eta^1\text{-dppm})(\eta^2\text{-dppm})]$ (**7**) | −0.41 | 14c |
| *cis*-$[Cr(CO)_2(dppe)_2]$ (**8**) | −0.70 | 15c |
| *trans*-$[Cr(CO)_2(dppe)_2]$ (**9**) | −1.06 | 15c |
| *cis*-$[Cr(CO)_2(dppm)_2]$ (**10**) | −0.66 | 11 |
| *trans*-$[Cr(CO)_2(dppm)_2]$ (**11**) | −1.30 | 11 |
| *cis*-$[Cr(CO)_2(pompom)_2]$ (**12**) | −0.36 | this work |
| *trans*-$[Cr(CO)_2(pompom)_2]$ (**13**) | −0.60 | this work |

[a] Potentials vs ferrocene.

Our results for $[Cr(CO)_4(PPh_3)_2]$ are somewhat ambiguous. Chemical or electrochemical oxidation did not produce the blue color reported by Bond and co-workers,[5] nor did oxidized solutions exhibit the reported EPR spectrum ($\langle g \rangle = 2.027$ and $\langle a^P \rangle = 18$ G). Indeed, no EPR spectrum attributable to a Cr(I) species was observed at temperatures down to 100 K. The failure to observe an EPR spectrum is consistent with the expected $^2E_g$ ground state expected for $[Cr(CO)_4(PPh_3)_2]^+$, but we are puzzled by the lack of color.

**Electrochemical Results.** Cyclic voltammograms were obtained for most of the compounds studied; oxidation half-wave potentials are listed in Table 2 together with literature values for some compounds for which our results were only semiquantitative.

Cyclic voltammograms of *cis*-$[Cr(CO)_2(pompom)_2]$ in $CH_2Cl_2$ are shown in Figure 2 with the half-wave potentials listed in Table 2. The primary oxidation approaches chemical reversibility at fast scans, but at slower scans, the reduction of the *trans* cation is observed on the reverse scan and the oxidation of the neutral *trans* isomer is observed on the second and subsequent scans. Digital simulations of the cyclic voltammograms, also shown in Figure 2, are consistent with the rate constant $k = 5 \pm 1$ $s^{-1}$ for the $cis^+ \rightarrow trans^+$ conversion, comparable to the rate constant for isomerization of the dppm analog ($k \approx 3$ $s^{-1}$ in $CH_2Cl_2$ at 20 °C) and considerably slower than that for the dppe compound ($k \approx 25$ $s^{-1}$).[15b] Isomerization of the dppm and dppe cations has been shown to occur with a negative entropy of activation, and an intramolecular twist mechanism was postulated. The similar rate found for the pompom complex supports this mechanism, since a significantly slower rate might have been expected if the process were dissociative.

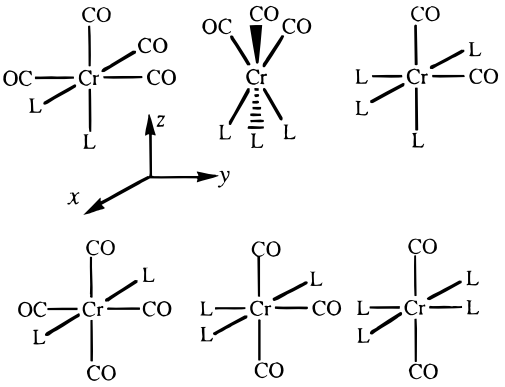


**Figure 3.** Molecules for which EHMO calculations were performed (L = $PH_3$, $P(OH)_3$), showing the coordinate system.

**Table 3. Bond Lengths (Å) Used in EHMO Calculations**

| | | | |
|---|---|---|---|
| Cr−C | 1.84,[a] 1.82[b] | P−H | 1.44 |
| Cr−P | 2.35,[a] 2.30[b] | P−O | 1.63 |
| C−O | 1.13,[a] 1.16[b] | O−H | 0.96 |

[a] Bond *trans* to CO. [b] Bond *trans* to P.

## Discussion

**Extended Hückel MO Calculations**. EHMO calculations[27] were performed for the molecules shown in Figure 3: *cis*- and *trans*-$[Cr(CO)_4L_2]$, *mer*- and *fac*-$[Cr(CO)_3L_3]$, and *cis*- and *trans*-$[Cr(CO)_2L_4]$ (L = $PH_3$, $P(OH)_3$). Bond lengths, given in Table 3, were based on the structures of *cis*-$[Cr(CO)_4(PH_3)_2]$,[28] *fac*-$[Cr(CO)_3$-

(27) EHMO calculations used the Alvarez collected parameters supplied with the CACHE software: CACHE Scientific, Beaverton, OR.

**Table 4. EHMO Predictions**

(a) Properties of HOMO's

| complex | *E*/eV | % Cr | overlap pop. Cr−CO | overlap pop. Cr−P |
|---|---|---|---|---|
| *cis*-[Cr(CO)$_4$(PH$_3$)$_2$] | −11.98 | 64.0 | 0.005,[a] 0.440[b] | 0.016 |
| *trans*-[Cr(CO)$_4$(PH$_3$)$_2$] | −11.84 | 68.3 | 0.206 | 0.000 |
| *fac*-[Cr(CO)$_3$(PH$_3$)$_3$] | −11.90 | 66.3 | 0.280 | 0.076 |
| *mer*-[Cr(CO)$_3$(PH$_3$)$_3$] | −11.61 | 74.8 | 0.010,[a] 0.618[b] | 0.006,[a] 0.022[b] |
| *cis*-[Cr(CO)$_2$(PH$_3$)$_4$] | −11.52 | 78.6 | 0.243 | 0.003,[a] 0.049[b] |
| *trans*-[Cr(CO)$_2$(PH$_3$)$_4$] | −11.16 | 93.6 | 0.000 | 0.009 |
| *cis*-[Cr(CO)$_4${P(OH)$_3$}$_2$] | −12.12 | 63.6 | 0.008,[a] 0.413[b] | 0.056 |
| *trans*-[Cr(CO)$_4${P(OH)$_3$}$_2$] | −12.05 | 66.6 | 0.224 | 0.051 |
| *fac*-[Cr(CO)$_3${P(OH)$_3$}$_3$] | −12.04 | 66.0 | 0.263 | 0.074 |
| *mer*-[Cr(CO)$_3${P(OH)$_3$}$_3$] | −11.77 | 74.5 | 0.016,[a] 0.521[b] | 0.042,[a] 0.071[b] |
| *cis*-[Cr(CO)$_2${P(OH)$_3$}$_4$] | −11.71 | 77.0 | 0.181 | 0.034,[a] 0.113[b] |
| *trans*-[Cr(CO)$_2${P(OH)$_3$}$_4$] | −11.40 | 92.2 | 0.000 | 0.050 |

(b) Isomerization Energies (eV)

| reacn | L = PH$_3$ | L = P(OH)$_3$ |
|---|---|---|
| *cis*-[Cr(CO)$_4$L$_2$] → *trans*-[Cr(CO)$_4$L$_2$] | −0.28 | −0.07 |
| *cis*-[Cr(CO)$_4$L$_2$]$^+$ → *trans*-[Cr(CO)$_4$L$_2$]$^+$ | −0.14 | −0.15 |
| *fac*-[Cr(CO)$_3$L$_3$] → *mer*-[Cr(CO)$_3$L$_3$] | +0.26 | −0.26 |
| *fac*-[Cr(CO)$_3$L$_3$]$^+$ → *mer*-[Cr(CO)$_3$L$_3$]$^+$ | −0.04 | −0.54 |
| *cis*-[Cr(CO)$_2$L$_4$] → *trans*-[Cr(CO)$_2$L$_4$] | +0.08 | −0.73 |
| *cis*-[Cr(CO)$_2$L$_4$]$^+$ → *trans*-[Cr(CO)$_2$L$_4$]$^+$ | −0.27 | −1.04 |

[a] Bond *trans* to CO. [b] Bond *trans* to P.

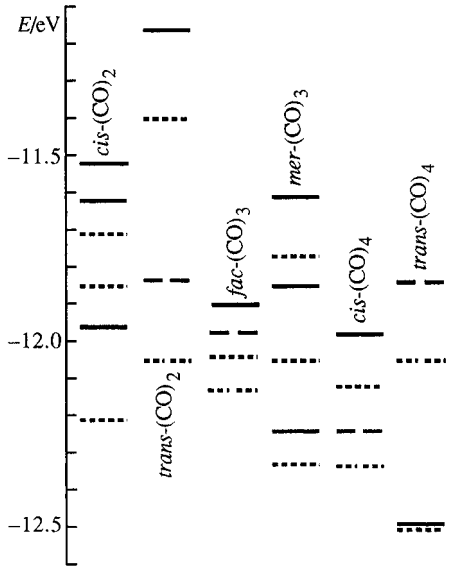


**Figure 4.** Energies of $\pi$-symmetry frontier orbitals of [Cr(CO)$_{6-n}$(PH$_3$)$_n$] (solid lines) and [Cr(CO)$_{6-n}${P(OH)$_3$}$_n$] (dashed lines).

(PH$_3$)$_3$],[29] and *cis*-[Cr(CO)$_2$(PH$_3$)$_4$],[30] adjusted slightly to approximately equalize the energies of *cis*- and *trans*-[Cr(CO)$_2$(PH$_3$)$_4$]. Bond angles were idealized 90, 109.5, and 180° angles. Lack of charge self-consistency is always a problem with EHMO calculations and is particularly serious for these calculations where negative charges develop on Cr and, with P(OH)$_3$ ligands, large positive charges develop on P. Nonetheless, useful insights are obtained from the calculations, the results of which are summarized in Table 4 and Figure 4.

On the whole, the results are similar to those of Mingos[8] for *mer*- and *fac*-[Mo(CO)$_3$(PH$_3$)$_3$] and *cis*- and *trans*-[Mo(CO)$_2$(PH$_3$)$_4$]. As expected from qualitative considerations, metal contributions to the frontier orbitals are the 3d orbitals of $\pi$ symmetry. For *trans*-[Cr(CO)$_2$L$_4$], *mer*-[Cr(CO)$_3$L$_3$], and *cis*-[Cr(CO)$_4$L$_2$], $\pi$-back-donation to CO stabilizes $d_{xz}$ and $d_{yz}$ relative to $d_{xy}$, the HOMO. For *trans*-[Cr(CO)$_4$L$_2$] and *cis*-[Cr(CO)$_2$L$_4$], $\pi$-back-bonding stabilizes $d_{yz}$ relative to $d_{xz}$ and $d_{xy}$, which are degenerate in the *trans* compound. For *fac*-[Cr(CO)$_3$L$_3$], the HOMO is $d_{z^2}$ with the degenerate $d_{x^2-y^2}/d_{xz}$ and $d_{xy}/d_{yz}$ hybrids lower in energy.

The predicted relative stability of isomers depends strongly on the bond lengths used in the calculations. With bond lengths adjusted to make *cis*-Cr(CO)$_2$(PH$_3$)$_4$ slightly more stable than the *trans* isomer, *trans*-[Cr(CO)$_4$(PH$_3$)$_2$], *fac*-[Cr(CO)$_3$(PH$_3$)$_3$], and *mer*-[Cr(CO)$_3${P(OH)$_3$}$_3$] are predicted to be the most stable, consistent with experimental results for other phosphine and phosphite complexes. *trans*-[Cr(CO)$_2${P(OH)$_3$}$_4$] is predicted to be more stable than the *cis* isomer, suggesting that *cis*-[Cr(CO)$_2$(pompom)$_2$] may be a kinetic, rather than thermodynamic, product of the synthesis. The Cr(I) *trans*-(CO)$_2$ and *mer*-(CO)$_3$ isomers are correctly predicted to be the most stable for both PH$_3$ and P(OH)$_3$ ligands.

Predictions of the oxidation half-wave potentials or the energies of the electron-transfer reactions of Schemes 1−3 are more reliable, since they depend only on the relative energies of the HOMO's and the HOMO energies are relatively insensitive to assumed bond lengths. A correlation of half-wave potentials with HOMO energies is shown in Figure 5; while substituent effects are not negligible, the major trends are well represented by calculations using the PH$_3$ and P(OH)$_3$ ligands. The electron-transfer reactions are predicted to be exoergic: −0.14 (PH$_3$) and −0.07 eV (P(OH)$_3$) for Scheme 1, −0.29 (PH$_3$) and −0.27 eV (P(OH)$_3$) for Scheme 2, −0.36 (PH$_3$) and −0.31 eV (P(OH)$_3$) for Scheme 3, in satisfactory agreement with experiment (see Table 2). These results can be understood when we consider the nature of the HOMO's. For the *cis* or *fac* isomers, the HOMOs make a significantly greater contribution to the Cr−CO and Cr−P overlap populations than those for the

(28) Guggenberger, L. S.; Klabunde, U.; Schunn, R. A. *Inorg. Chem.* **1973**, *12*, 1143.
(29) Huttner, G.; Schelle, S. *J. Organomet. Chem.* **1973**, *47*, 383.
(30) Huttner, G.; Schelle, S. *J. Cryst. Mol Struct.* **1971**, *1*, 69.

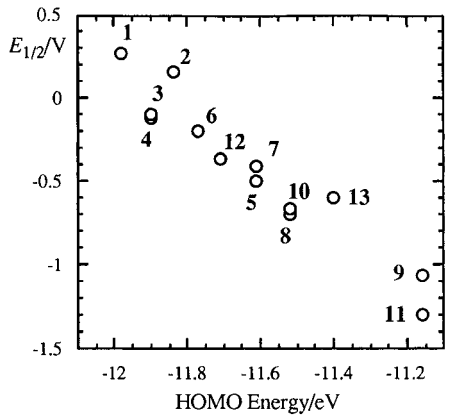


**Figure 5.** Correlation of electrochemical oxidation potentials with computed HOMO energies. The numbers identify the compounds of Table 2.

*trans* or *mer* isomers. Since the average overlap populations are comparable in the Cr(0) isomers, oxidation results in a greater loss in metal−ligand overlap population for the *cis* and *fac* isomers, leading to the preference for *trans* or *mer* in the Cr(I) complexes. Related to this is the greater HOMO metal character for the *trans* and *mer* isomers. Thus, there is a significant change in charge distribution associated with the electron-transfer processes, consistent with the observed solvent dependence of $\Delta G°$; for example, for the $[Cr(CO)_2(dppe)_2]$ system,[15c] $\Delta G°$ ranges from −0.325 eV (toluene) to −0.375 eV (acetonitrile).

In general, the EHMO calculations show decreases in the Cr−P $\sigma$-overlap population and increases in the Cr−P $\pi$-overlap population for $P(OH)_3$ compared with $PH_3$, consistent with the expected lower $\sigma$-basicity and greater $\pi$-acidity of phosphites. Small decreases in the Cr−CO $\pi$-overlap population are found when $PH_3$ is replaced by $P(OH)_3$ in the calculations. In other words, phosphite ligands compete with carbonyls for $\pi$-electron density. In the *fac* conformation, there is direct competition in all MO's of $\pi$ symmetry, whereas *mer* complexes have 3 P acceptors competing with a single CO for $d_{xy}$ electrons, 2 P's and 2 CO's for $d_{xz}$ electrons, and 1 P and 3 CO's for $d_{yz}$ electrons. This variety allows for greater average Cr−P and Cr−CO $\pi$ interactions in the *mer* conformation compared with *fac* and may explain the preference for *mer* by tris(phosphites) and -(phosphonites) in both the 0 and +1 oxidation states.

The predicted metal spin densities for the Cr(I) complexes given in Table 4 are significantly greater than the values obtained, ca. 0.35, from analysis of the $^{51}V$ hyperfine anisotropy for *trans*-$[V(CO)_4(PMe_3)_2]$[7f] and *fac*-$[V(CO)_3(PMe_3)_3]$.[7g,31] The reported values are almost certainly low, largely because the dipolar coupling parameter used to compute the spin densities, $P = 146 \times 10^{-4}$ cm$^{-1}$,[32] was computed from Hartree−Fock wave functions for the V $d^3s^2$ configuration. With the more realistic $d^5$ configuration, $P = 106 \times 10^{-4}$ cm$^{-1}$,[33] spin densities on the order of 0.5 are obtained. Furthermore, the higher nuclear charge for Cr would be expected to lead to greater metal character in the frontier MO's (EHMO calculations suggest an increase of *ca.* 10%). Thus, the calculated spin densities for the Cr(I) complexes are qualitatively consistent with experimental results for the isoelectronic V(0) complexes.

***g*-Matrix Components**. For a SOMO where the metal contribution is $d_{xy}$

$$|\mathrm{SOMO}\rangle = a\langle|xy\rangle + ... \quad (1)$$

the components of the **g**-matrix are given by eqs 2, where $g_e$ is the free-electron $g$ value, $\zeta$ is the Cr spin−orbit coupling constant, $E_0 - E_m$ is the difference in energy between the SOMO and the $m$th molecular orbital, and $c_{m,i}^2$ is the LCAO coefficient of atomic orbital $i$ in molecular orbital $m$.

$$g_{xx} = g_e + \zeta \sum_{m \neq 0} \frac{a^2 c_{m,xz}^{\ 2}}{E_0 - E_m} \quad (2a)$$

$$g_{yy} = g_e + \zeta \sum_{m \neq 0} \frac{a^2 c_{m,yz}^{\ 2}}{E_0 - E_m} \quad (2b)$$

$$g_{zz} = g_e + \zeta \sum_{m \neq 0} \frac{4a^2 c_{m,x^2-y^2}^{\ 2}}{E_0 - E_m} \quad (2c)$$

Stabilizations of $d_{xz}$ and $d_{yz}$ should be identical for *trans*-$[Cr(CO)_2L_4]^+$, since each orbital interacts with the two CO ligands; thus, we expect $c_{m,xz}^2 = c_{m,yz}^2$ and $g_{xx} = g_{yy} > g_e$. Similarly, in *cis*-$[Cr(CO)_4L_2]^+$ $d_{xz}$ and $d_{yz}$ each interact with three CO ligands and we expect $g_{xx} = g_{yy} > g_e$. With *mer*-$[Cr(CO)_3L_3]^+$, $d_{xz}$ interacts with two, and $d_{yz}$ interacts with three CO's so that the $d_{xz}$/$d_{yz}$ degeneracy is lifted. Thus we expect the MO with $d_{yz}$ character to be lowest in energy so that $g_{xx} > g_{yy} > g_e$. In all three cases, $d_{x^2-y^2}$ is involved in metal−ligand $\sigma$-bonding and antibonding MO's, well separated in energy from the SOMO so that $g_{zz}$ should be close to $g_e$.

The description for *fac*-$[Cr(CO)_3L_3]^+$ is complicated by the fact that, in $C_{3v}$ symmetry, the $t_{2g}$ set is $d_{z^2}$ ($a_1$) and $(2/3)^{1/2}d_{x^2-y^2} - (1/3)^{1/2}d_{xz}$, $(2/3)^{1/2}d_{xy} + (1/3)^{1/2}d_{yz}$ (e). The e set is more involved in $\pi$-back-donation to the CO ligands and thus is stabilized relative to $d_{z^2}$, which is expected to be the dominant contributor to the SOMO with LCAO coefficient $a$. Spin−orbit coupling of $d_{z^2}$ with the degenerate $d_{xz}$ and $d_{yz}$ contributions to the other MO's leads to an axial **g**-matrix with $g_\perp$ given by eq 3, where $c_{m,d_e}$ is the LCAO coefficient of one of the e set metal hybrids in the $m$th MO.

$$g_\perp = g_e + \zeta \sum_{m \neq 0} \frac{a^2 c_{m,d_e}^{\ 2}}{E_0 - E_m} \quad (3)$$

These predictions are largely fulfilled by the EPR results. Two of the four *mer* complexes—$L_3 = (PMe_3)_3$ and $(PPhMe_2)_3$—have rhombic **g**-matrices with $g_{xx} \neq g_{yy}$, while the other two—$L_3 = \{PPh(OMe)_2\}_3$ and ($\eta^1$-dppm)-($\eta^2$-dppm)—have approximately axial **g**-matrices. The *fac* complexes—$L_3$ = triphos, $(PPhMe)_3$—have axial **g**-matrices as expected. The qualitative theory predicts axial **g**-matrices for *cis*-$[Cr(CO)_4L_2]^+$ and *trans*-$[Cr(CO)_2L_4]^+$. The nearly axial **g**-matrices found for the

(31) The chemical instability of *fac*-$[Cr(CO)_3(PMe_3)_3]^+$ [22] suggests that the V(0) species detected by McCall et al.[7g] was the *mer* isomer. As we see in the present work, an approximately axial **g** matrix and approximately equivalent $^{31}P$ couplings are not necessarily indicative of *fac* stereochemistry. In any case, the frozen-solution spectrum was misinterpreted and the reported $^{31}P$ hyperfine anisotropy is certainly much too large.

(32) Morton, J. R.; Preston, K. F. *J. Magn. Reson.* **1978**, *30*, 577.

(33) Rieger, P. H. *J. Magn. Reson.* **1997**, *124*, 140.

dppe complexes are consistent with the small distortions from $C_{2v}$ and $D_{4h}$ symmetry introduced by the $C_2H_4$ bridge. The departure from axial symmetry is much larger for *trans*-$[Cr(CO)_2(dppm)_2\}^+$ and *trans*-$[Cr(CO)_2(pompom)_2]^+$, suggesting much larger distortions. Relatively small distortions associated with the dppm ligand in *trans*-$[Mn(CO)(CN)(dppm)_2]^+$ result in a significant off-diagonal *xz* component in the **g**-matrix, leading to displacement of the **g**-matrix principal axes from the molecular axes;[34] a similar effect in *trans*-$[Cr(CO)_2(dppm)_2]^+$ probably accounts for the departure from axial symmetry. The magnitudes of the **g**-matrix components are qualitatively consistent with the energy level diagrams shown in Figure 4.

**$^{31}$P Hyperfine Coupling**. In general, we expect the isotropic $^{31}$P hyperfine couplings to arise from P 3s character in the SOMO or from polarization of inner-shell P s orbitals by spin density on the metal or in P 3p orbitals. This sum of contributions can be expressed by eq 4. For an ideal *trans*-$(CO)_4$ complex ($D_{4h}$ symmetry), the P atoms would lie on a nodal plane of the $d_{xy}$ orbital and the first term of eq 4 would be negligible. However, since $A^P_s$ is large, 4438 × $10^{-4}$ cm$^{-1}$,[32] even small departures from ideality can lead to a large correction.

$$\langle \mathbf{A}^P \rangle = A^P{}_s \rho_P{}^s + Q^P{}_{Cr} \rho_{Cr}{}^{3d} + Q^P{}_p \rho_P{}^{3p} \qquad (4)$$

The second term of eq 4 is probably the largest in magnitude for the $^{31}$P couplings reported here. Thus, the couplings are generally larger for the *trans*-$(CO)_2$ complex than for the *mer*-$(CO)_3$ or *cis*-$(CO)_2$ complexes, consistent with the larger metal spin density predicted by EHMO calculations, (Table 4). The larger couplings observed for the phosphonites (phosphite $^{31}$P couplings are generally larger in magnitude than analogous phosphine couplings) compared with the phosphines may be due in part to the larger P 3p spin density arising from $\pi$-back-donation and the subsequent contribution of the third term of eq 4, but, more likely, the parameter $Q^P{}_{Cr}$ may be larger in magnitude for the phosphonites than for the phosphines.[35]

The unique P atom in the *mer* complexes has a somewhat larger coupling than does the equivalent pair. Assuming $C_{2v}$ symmetry, P 3s character is forbidden for the unique P atom, which lies on the plane of symmetry, but is allowed for the equivalent pair. Indeed EHMO calculations predict a 3s spin density of 0.0008 for these atoms, corresponding to a hyperfine coupling contribution of about 4 × $10^{-4}$ cm$^{-1}$, comparable to the observed difference between the two $^{31}$P couplings and consistent if $Q^P{}_{Cr}$ is negative as expected. The lower symmetry of *mer*-$[Cr(CO)_3(\eta^1\text{-dppm})(\eta^2\text{-dppm})]^+$ [36,37] allows for P 3s character for the unique phosphorus atom as well as the nominally equivalent pair, consistent with the smaller observed unique $^{31}$P coupling. Assuming that *mer*-$[Cr(CO)_3(PMe_3)_3]^+$ is close to true $C_{2v}$ symmetry (and thus that there is no P 3s contribution to the SOMO for the unique phosphorus atom), that the third term of eq (4) may be neglected, and that the EHMO prediction of metal spin density is correct, we obtain an estimate for the polarization parameter, $Q^P{}_{Cr} \approx -38 \times 10^{-4}$ cm$^{-1}$. This is considerably larger in magnitude than the observed coupling for the *trans*-$(CO)_2$ complexes, where EHMO calculations predict a metal spin density of 0.94. However, the dppm and dppe chelate rings reduce the symmetry and the P−Cr−P bond angles are considerably smaller than 90°,[34,38] permitting P 3s admixture and a reduction in the magnitude of the observed couplings. It is probably significant that *trans*-$[Cr(CO)_2(dppm)_2]^+$, where the distortion is greater, gives a significantly smaller coupling than is found for the dppe analog. If this explanation is correct, one would expect a significantly larger coupling for the unknown complex *trans*-$[Cr(CO)_2(PMe_3)_4]^+$.

The $^{31}$P hyperfine matrices are nearly isotropic in all cases, but this may be more apparent than real. The frozen-solution spectra are not always well-resolved, but even if they were, the expected anisotropies are small compared with $|\langle A^P \rangle|$. Furthermore, because the **g**-matrix anisotropy is much greater than that of the $A^P$ matrix, observed spectral features correspond to orientations of the magnetic field along one of the **g**-matrix principal axes; thus the full hyperfine anisotropy may not be observed directly. Even if spectral resolution were better, analysis of the anisotropy would be challenging. Anisotropy is expected through dipolar coupling of the $^{31}$P nuclei with spin density on Cr (major axis along the Cr−P bond) or in a P 3p orbital (major axis perpendicular to the Cr−P bond if the P 3p orbital is involved in a $\pi$ interaction). The **g**-matrix principal axes are determined by the symmetry of the complexes. Assuming that *cis*-$[Cr(CO)_4L_2]^+$ and *mer*-$[Cr(CO)_3L_2]^+$ have approximate $C_{2v}$ symmetry and that *trans*-$[Cr(CO)_2L_4]^+$ has approximate $D_{4h}$ symmetry, the **g**-matrix axes are necessarily along the *x*, *y*, and *z* molecular axes. However, for the *cis*-$L_2$ and *trans*-$L_4$ complexes, the Cr−P bond vectors lie approximately midway between the *x* and *y* axes; furthermore, the **g** matrix *x* and *z* axes in the *trans*-$L_4$ complexes are probably significantly displaced from the molecular axes, particularly for dppm.[34] Only in the case of *mer*-$[Cr(CO)_3L_3]^+$ are the **g**-matrix and $A^P$-matrix axes coincident, but, because of the inequivalence of the $^{31}$P atoms, resolution is not good enough to justify detailed analysis. These problems were overcome in the analysis of the $^{31}$P hyperfine anisotropies in spectra of $[Cr(CO)_2L(\eta\text{-}C_6Me_6)]^+$, and some of the insights we had hoped for in the present work are reported elsewhere.[35]

OM970252H

(34) Carriedo, G. A.; Connelly, N. G.; Perez-Carreno, E.; Orpen, A. G.; Rieger, A. L.; Rieger, P. H.; Riera, V.; Rosair, G. M. *J. Chem. Soc., Dalton Trans.* **1993**, 3103.

(35) Castellani, M. P.; Connelly, N. G.; Pike, R. D.; Rieger, A. L.; Rieger, P. H. *Organometallics* **1997**, *16*, 4369.

(36) The P−Cr−P bond angles in this complex are 71.1° (chelate ring) and 106.8°.[37]

(37) Colton, R.; Hoskins, B. F.; McGregor, K. *Aust. J. Chem.* **1987**, *40*, 1471.

(38) The average P−Cr−P chelate ring bond angle in $[Cr(CO)_2(Me_2PCH_2CH_2PMe_2)_2]$ is 83.6°.[10]